Proceedings of the 11th Brazilian Congress of Thermal Sciences and Engineering – ENCIT 2006
Braz. Soc. of Mechanical Sciences and Engineering – ABCM, Curitiba, Brazil, Dec. 5-8, 2006

Paper CIT06-0432

Numerical Solution of 2-Dimensional Linearized Euler Equations for Acoustic Waves in Flow

Leandro Dantas de Santana
SMM – EESC – USP Av. Trabalhador Sancarlense, 400, CEP:13566-590 São Carlos - SP
dantas@sc.usp.br

Leandro Franco de Souza
SME – ICMC – USP Av. Trabalhador Sancarlense, 400, CEP:13560-970 São Carlos - SP
lefraso@icmc.usp.br

Abstract. *Aeroacoutics is a relatively new area of study derived from Mechanic of Fluids. Its study had made fantastic advances on the last fifteen years. The noise levels requirements for certificating an aircraft are gradually more restrictive and the study in this area is increasing. This industrial need, brought attention of academic community to this field. In this way this paper shows a review and comparison of the most used optimized finite difference with a 4th order Runge-Kutta scheme. A new finite difference scheme, based on spectral optimization is proposed. A 2-dimensional linearized Euler code is verified. For verification a benchmark case of a Gaussian pulse propagation was performed. As boundary conditions the non-reflective Perfectly Matched Layer (PML) zone is implemented and analyzed. The results shows that the proposed finite difference scheme gives better results in 1D propagation than in 2D propagation. The analysis of the PML zone shows that the reflections are very small.*

keywords: *Computational Aeroacoustics, Linearized Euler equations, Low dispersion, Low dissipation, Perfectly Matched Layer*

1. Introduction

The actual concern with environmental problems caused by noise generation in regions near airports imposed more restrictives environmental laws. These restrictions are the more severe noise criteria for certification of aircrafts. There are estimates that, if the Brazilian aircraft industry keeps its actual state of technology, in the next 15 years the most of the Brazilians airplanes will not be able to operate in the most important Europe and USA airports.

Computational Aeroacoustics (CAA) is the area that studies the noise generated aerodynamically. The most common approach of CAA is to divide the problem on two secondary problems. The first one, concerns on simulating the airflow using traditional CFD techniques: RANS, DNS, LES, etc. The second problem is to study the acoustic field for a given airflow. in this problem the viscosity effects are non considered and the Navier-Stokes equations are rewritten in a wave form.

The first research in the area of aeroacoustics began with two seminal papers of Sir James Lighthill, 1952; Lighthill, 1954. Lighthill focus was on find sources of sound in turbulent flows. This was achieved by an acoustic analogy. The basic idea of this approach is to consider the viscosity terms negligible and rewrite the Navier-Stokes equations on the form of compressible Euler's equations. At this way the left-hand side consisted of a second-order wave-equation, representing the sound propagation. All other terms were moved to the right hand side and were considered sources. The resulting wave equation, for the density ρ, is:

$$\frac{\partial^2 \rho}{\partial t^2} + c_0^2 \frac{\rho}{\partial x_j \partial x_j} = \frac{\partial T_{ij}}{\partial x_i \partial x_j}, \tag{1}$$

where c_0 is the ambient sound speed and $T_{ij} = \rho v_i v_j + (p - \rho c_0^2)\delta_{ij} - \tau_{ij}$ is the Lighthill stress tensor, and v_i, p, τ_{ij} and δ_{ij} are the velocity, pressure, viscous stress tensor and Kronecker delta, respectively.

An extension of Lighthill's acoustic analogy, to incorporate the effect of solid surfaces was published by Curle, 1955 and generalized by Williams, 1963. The effect of convection on directivity was introduced by Williams, 1969. From the middle sixties to the early nineties all aeroacoustics development were theoretical. On nineties Tam and Webb, 1993 published an optimized finite difference scheme and simulated linearized Euler Equations submitted to a Gaussian pulse on pressure and density fields and re-stated the aeroacoustic study.

One of the most significant difficulties of aeroacoustic solutions is to represent correctly the aeroacoustic quantities. Normally these quantities are so small when compared with fluid dynamic quantities that for

traditional CFD codes the acoustic effects could be neglected. To transport correctly the aeroacoustic quantities, the Navier-Stokes equations can be simplified. The first simplification is to neglect the viscosity terms, since the Reynolds numbers given by:

$$Re_\lambda \approx \frac{|\rho\frac{\partial u'}{\partial t}|}{|\mu\frac{\partial^2 u'}{\partial x^2}|} \approx \frac{\lambda^2 f}{\mu/\rho}, \tag{2}$$

for these cases are very large. Here λ is the wave length, f is the frequency and μ/ρ is the kinematic viscosity. For a typical problem of sound propagation in air these parameters are:

- $\nu = \mu/\rho = 1.4 \times 10^{-5} m^2/s$;
- $f = 1kHz$;
- $c_0 = 340m/s$;
- $\lambda = c_0/f = 34.4m$ and

these values leads to a typical Reynolds number of aeroacoustic problems of $Re_\lambda = 1 \times 10^7$. Using the fact that the Reynolds number is so high, the viscosity terms are very small when compared with dynamic terms, that the viscosity terms can be neglected. This simplification leads to the Euler equations. The second simplification adopted here is the linearization of the Euler equations. This simplification can be done without loss of physical behavior, since the amplitude of the disturbances are very small.

The present paper study the numerical propagation of a 1D and 2D waves. The equations adopted for these verifications are the 1D hyperbolic equation and 2D Linearized Euler Equations (LEE). The discretizations are done by Optimized Finite Difference schemes (Tam and Webb, 1993; Bogey and Bailly, 2004) and a proposed Spectral Optimized SO finite difference scheme. A 4th order 4 steps Runge-Kutta scheme was adopted for time integration. Effects of reflections at the boundaries are tested with Perfectly Matched Layer (PML) zone.

The work is divided as follows: the first section shows formulation used; the finite-difference schemes, the time integration scheme and the PML zone are shown in the second section; the third section shows the Numerical results and the last section shows the conclusions of the present study.

2. Formulation

This section was divided in two subsections: 1D transport equation and 2D transport equation. Both formulations were used in the current study. The details of each formulation is given bellow.

2.1. 1D transport equation

To analyze one dimensional characteristics of finite difference schemes a wave transport, the 1D hyperbolic equation used was:

$$\frac{\partial f}{\partial t} + \frac{\partial f}{\partial x} = 0, \tag{3}$$

where the initial condition adopted was:

$$f(x, t = 0) = \sin\left(\frac{2\pi x}{30}\right) \qquad \text{for} \qquad 10 \leq x \leq 30, \tag{4}$$

for $x < 10$ and $x > 30$ the value of $f(x, t = 0) = 0$ was settled.

2.2. 2D transport equation

The high Reynolds number of acoustic terms suggest that viscous terms are negligible when compared with others terms. Another important fact to be considered is that the order of the terms related to acoustic propagation is very small when compared with the order of the terms of the fluid dynamic motion. This leads to a linearization on full Euler equations. Colonius *et al.*, 1993 shows that this approach solves the problem, with a smaller computational cost, without loosing the quality of the numerical solution.

A way to improve the generality of the computational code simulation is to implement the non-dimensional form of LEE. To perform this we introduce the non-dimensional scales: Length scales $= \Delta x = \Delta y$, Velocity scales $= c_0$, Time scales $= \Delta x/c_0$, Density scales $= \rho_0$, Pressure scales $= \rho_0 c_0^2$, where $\Delta x = \Delta y$ are the distance between two consecutive points in the x and y directions, respectively, and c_0 is the sound velocity given by $c_0 = \sqrt{\gamma p_0/\rho_0}$. Using these parameters, the non-dimensional LEE can be written as:

$$\frac{\partial \mathbf{u}}{\partial t} + \mathbf{A}\frac{\partial \mathbf{u}}{\partial x} + \mathbf{B}\frac{\partial \mathbf{u}}{\partial y} = \mathbf{H}^*, \tag{5}$$

where $\mathbf{H}^*$ is the non-dimensional source term, and

$$\mathbf{u} = \begin{pmatrix} \rho' \\ u' \\ v' \\ p' \end{pmatrix}, \qquad \mathbf{A} = \begin{pmatrix} M & 1 & 0 & 0 \\ 0 & M & 0 & 1 \\ 0 & 0 & M & 0 \\ 0 & 1 & 0 & M \end{pmatrix}, \qquad \mathbf{B} = \begin{pmatrix} 0 & 0 & 1 & 0 \\ 0 & 0 & 0 & 0 \\ 0 & 0 & 0 & 1 \\ 0 & 0 & 1 & 0 \end{pmatrix}, \tag{6}$$

are the respectively matrices, that are used for computational simulation for next sections.

2.2.1. The analytical solution for LEE

This subsection presents the exact solution of the test case of a Gaussian pulse on density and pressure fields used at the present paper. This solution is used on future section to analyze characteristics of the finite difference schemes.

Tam and Webb, 1993 presents the analytical solution, based on Green function presented by Williams, 1969, for the LEE on a Cartesian grid with constant mesh size when the initial condition is a Gaussian pulse on pressure and density field. This initial condition is defined as:

$$\begin{aligned} t &= 0, \\ p &= \rho = \epsilon_1 e^{-\alpha_1 r^2}, \\ u &= 0, \\ v &= 0, \end{aligned} \tag{7}$$

and the boundary conditions are:

$$\begin{aligned} \text{at} \quad x = X_{max}, \quad y = Y_{min} \quad \text{and} \quad y = Y_{max} \quad &: \quad p = 0, \\ \text{at inflow} \quad x = X_{min} \quad &: \quad p = \rho = v = 0, \end{aligned} \tag{8}$$

applying these physical boundary conditions, one could reach the exact solution for the velocity components (u and v) and the pressure and density field (p, ρ) as:

$$u(x,y,t) = \frac{\epsilon_1 (x - Mt)}{2\alpha_1 \eta} \int_0^\infty e^{-\xi^2/4\alpha_1} \sin(\xi t) J_1(\xi\eta) \xi d\xi, \tag{9}$$

$$v(x,y,t) = \frac{\epsilon_1 y}{2\alpha_1 \eta} \int_0^\infty e^{-\xi^2/4\alpha_1} \sin(\xi t) J_1(\xi\eta) \xi d\xi, \tag{10}$$

$$p(x,y,t) = \rho = \frac{\epsilon_1}{2\alpha_1} \int_0^\infty e^{-\xi^2/4\alpha_1} \cos(\xi t) J_0(\xi\eta) d\xi, \tag{11}$$

where $\eta = [(x - Mt)^2 + y^2]^{1/2}$, J_0 e J_1, and J_0 and J_1 are respectively, the Bessel functions of first kind and zeroth and first order, respectively.

3. Numerical method

In the present section the optimized finite difference schemes, the time integration method and the PML zone are shown. The equations adopted here (1D Hyperbolic equation and LEE) needs only the evaluation of first order derivatives, and the current paper concerns only the finite difference schemes that treat these derivatives. There are two main kinds of finite difference schemes: explicit schemes and implicit ones. The implicit schemes uses smaller stencils when compared with explicit ones, for the same truncation error, with the drawback to obtain the inverse of a coefficient matrix. Explicit schemes, otherwise, needs greater stencils. This can be a problem near boundaries, but as will be shown in a future section, the application of PML zone reduces the importance of the non-centered finite difference technique.

In present section, the first subsection presents a general presentation of finite difference schemes, and its first subsection presents the DRP and FDo finite difference schemes, the next one presents the proposed SO finite difference scheme. The next subsection presents the Runge-Kutta scheme adopted. The last subsection shows the details of the PML zone.

3.1. Finite difference schemes

The standard approach finite difference method evaluates the spatial derivative of a function in a uniform grid points equally spaced by Δx using the following approximation, for a symmetric (2N+1)-point stencil, one can write:

$$\frac{\partial f}{\partial x}(x) \simeq \sum_{j=-N}^{N} a_j f(x + j\Delta x) \tag{12}$$

where a_j are the weight coefficients, defined for a given finite difference method. To reach great orders one could find greater stencils. Tam, 1995 shows that traditional finite difference schemes are not the better approximation for aeroacoustics derivatives calculations. The following section shows two optimized finite difference schemes presented in literature.

3.1.1. DRP and FDo finite difference schemes

Tam and Webb, 1993 shows that the improvement of formal order on finite difference scheme is not as important as its spectral characteristics. Looking for better characteristics for their finite difference schemes, Tam and Webb, 1993 applied the Fourier transform to Eq. 12 and minimized the spectral absolute error in the range of $0 \leq \pi/2$. By doing that they obtained optimized schemes called Dispersion-Relation-Preserving (DRP) finite difference method.

Bogey and Bailly, 2004 present an improvement to DRP method. They show that a better way to obtain the finite difference coefficients is not to minimize the absolute error, but to minimize the relative absolute error. They adopted the range $\pi/16 \leq \pi/2$, for schemes of 9 and 11 points and $\pi/16 \leq 3\pi/5$ for schemes of 13 points. Their proposed scheme was called Finite Difference Optimized (FDo). Tab. 1 presents the coefficients of this both methods.

Table 1: Coefficients for finite difference schemes, where $a_0 = 0$ and $a_j = -a_{-j}$.

Coef.	DRP	FDo9p	FDo11p	FDo13p
a_1	0.79926643	0.8415701254	0.8727569939	0.9076465913
a_2	-0.18941314	-0.2446786317	-0.2865111739	-0.3370483932
a_3	0.02651995	0.0594635847	0.0903200012	0.1334428853
a_4		-0.0076509040	-0.0207794058	-0.0452464802
a_5			0.0024845946	0.0111692941
a_6				-0.0014565017

3.1.2. Spectral Optimized finite difference scheme

A new finite difference scheme is proposed in the current work. It is based on Spectral Optimization (SO). This method is based on Lele, 1992 technique of optimization for compact schemes, and was adapted here to optimize explicit finite difference methods.

Differently from Tam and Webb, 1993 and Bogey and Bailly, 2004, the technique does not try to optimize an objective function. It is defined a family of straight forward constraints that defines the formal order of the scheme, and find a some points on spectrum where the relation $k'\Delta x = k\Delta x$ results in a good spectral characteristics.

Using this approach, the $k'\Delta x = k\Delta x$ condition, for centered explicit schemes with $2N + 1$ stencil points can be rewritten as:

$$k = 2 \times \sum_{j=0}^{M} a_j \sin(jk), \tag{13}$$

to best representative the condition presented in Eq. (13) and the constraint condition the following matrix

form is presented:

$$\begin{pmatrix} \sin m & \sin 2\times m & \cdots & \sin k\times m \\ \sin n & \sin 2\times n & \cdots & \sin k\times n \\ \vdots & \vdots & \ddots & \vdots \\ \sin z & \sin 2\times z & \cdots & \sin k\times z \\ CCtt_1 1 & CCtt_1 2 & \cdots & CCtt_1 k \\ \vdots & \vdots & \ddots & \vdots \\ CCtt_k 1 & CCtt_k 2 & \cdots & CCtt_k k \end{pmatrix} \times \begin{pmatrix} a_1 \\ a_2 \\ \vdots \\ a_j \\ a_l \\ \vdots \\ a_k \end{pmatrix} = \begin{pmatrix} m \\ n \\ \vdots \\ z \\ 0 \\ \vdots \\ 0 \end{pmatrix}, \tag{14}$$

where $m, n, \ldots, z$ are points conveniently choose on spectrum where the relation $k'\Delta x = k\Delta x$ is valid. $CCtt_u v$ are the coefficient of the constraint condition and a_j are the finite difference coefficients.

To define a sixth order finite difference scheme with 11 stencil points the values of m, n, p, q and r adopted are:

$$\begin{aligned} m = 0.2\pi, \quad n = 0.35\pi, \quad p = 0.45\pi, \\ q = 0.5\pi, \quad r = 0.6\pi, \end{aligned} \tag{15}$$

applying this method, the sixth order SO coefficients are:

$$\begin{aligned} a(1) = 0.89862767688255, \quad a(2) = -0.32385996447943, \quad a(3) = 0.12047995924059, \\ a(4) = -0.03334363299405, \quad a(5) = 0.00458628520861. \end{aligned} \tag{16}$$

3.2. Runge-Kutta scheme

Runge-Kutta schemes are by far the most commonly used scheme for time integration on computational aeroacoustics. The time evolution equation can be written as:

$$\frac{\partial \mathbf{U}}{\partial t} = F(\mathbf{U}), \tag{17}$$

where $\mathbf{U}$ represents the vector containing the solution values of the spatial functions and finite difference derivatives. An explicit low-storage *p-stage* Runge-Kutta scheme advance the solution from time level t_n to $t_n + \Delta t$ in the form:

$$\begin{aligned} u^0 &= u^n, \\ u^l &= u^n + \alpha_l \Delta t F(u^{u^{l-1}}) \quad \text{for l=1,..,p}, \\ u^{n+1} &= u^p. \end{aligned} \tag{18}$$

To analyze and compare the effect of the accouplement of the Runge-Kutta scheme with the finite difference scheme the Figs. 1 and 2 presents the modulus of the amplification factor of the 4^{th}-order Runge-Kutta scheme, for the DRP and SO finite difference schemes, respectively. Comparing the the Figs. 1 one can note that for

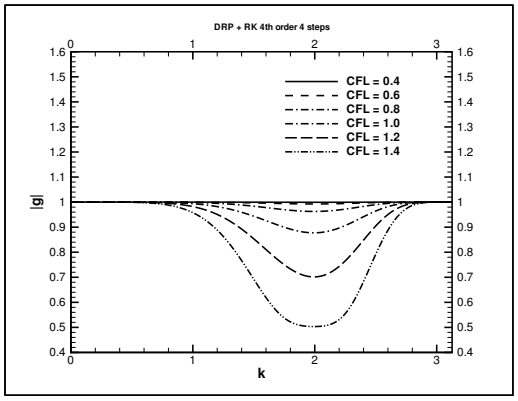

Figure 1: Dissipation factor of a RK 4^{th}-order with DRP method.

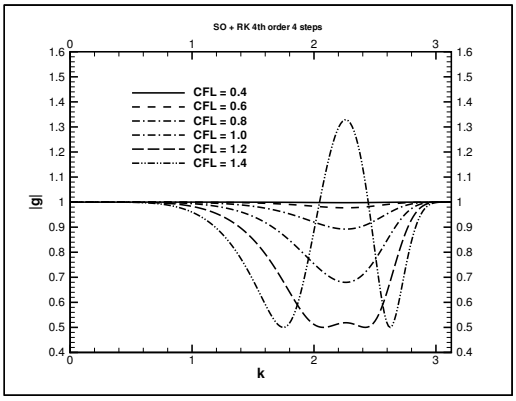

Figure 2: Dissipation factor of a RK 4^{th}-order with SO method.

small wave-number the two schemes gives similar answers. As the CFL number increases some dissipation is noted. DRP scheme is dissipative but stable for all wave-numbers and CFL numbers on the range analyzed, and SO scheme can be unstable for CFL > 1.3.

3.3. Numerical treatment of the boundaries

Nowadays one of the most relevant topic of discussion on computational aeroacoustics is the correct used of numerical schemes at and near the boundaries of the computational domain. A good numerical scheme on the boundary should be able to absorb all disturbances (far-field boundary condition) without any reflection to the interior of the domain. There are several schemes on literature, one scheme that seems to be the best of them is presented by Hu, 2001. This scheme applies a dumping zone near the boundary of the computational domain. The main advantage of this technique when compared with others is that this approach do not need stretching on the mesh near the boundary and its computational cost is not so high. The equation for this scheme is:

$$\frac{\partial \mathbf{u}}{\partial t} + \mathbf{A}\frac{\partial \mathbf{u}}{\partial x} + \mathbf{B}\frac{\partial \mathbf{u}}{\partial y} + \sigma_y \mathbf{A}\frac{\partial \mathbf{q}}{\partial x} + \sigma_x \mathbf{B}\frac{\partial \mathbf{q}}{\partial y} + (\sigma_x + \sigma_y)\mathbf{u} + \\ + \sigma_x \sigma_y \mathbf{q} + \frac{\sigma_x M}{1 - M^2}\mathbf{A}(\mathbf{u} - \sigma_y \mathbf{q}) = 0, \tag{19}$$

where σ_x and σ_y are dumping factors in the x and y directions, respectively, and $\mathbf{q}$ is a vector of auxiliary variables. Analyzing the Eq. 19 one could note that if $\sigma_x = \sigma_y = 0$ we go back to equation to LEE on its non dimensional for (Eq. 5). Hu, 2001 defines the dumping factors as:

$$\sigma_x = \sigma_m (1 - M^2) |\frac{x - x_l}{D}|^\beta, \quad \sigma_y = \sigma_m |\frac{y - y_l}{D}|^\beta, \tag{20}$$

where x_l and y_l represents the set of points where the PML zones starts and D is the length of the PML zone. Completing the procedure, one could note that in the horizontal region of PML zone $\sigma_x = 0$ and for the vertical region of PML zone $\sigma_y = 0$. Leading to some simplifications on PML equations represented respectively by:

$$\frac{\partial \mathbf{u}}{\partial t} + \mathbf{A}\frac{\partial \mathbf{u}}{\partial x} + \mathbf{B}\frac{\partial \mathbf{u}}{\partial y} + \sigma_x \mathbf{B}\frac{\partial \mathbf{q}}{\partial y} + \sigma_x \mathbf{u} + \frac{\sigma_x M}{1 - M^2}\mathbf{A}\mathbf{u} = 0, \tag{21}$$

$$\frac{\partial \mathbf{u}}{\partial t} + \mathbf{A}\frac{\partial \mathbf{u}}{\partial x} + \mathbf{B}\frac{\partial \mathbf{u}}{\partial y} + \sigma_y \mathbf{A}\frac{\partial \mathbf{q}}{\partial x} + \sigma_y \mathbf{u} = 0. \tag{22}$$

Hu, 1996 shows that the choice of the parameters σ_m and β have to be according to the length of the computational domain. He also shows that, for a uniform square mesh with a minimal dimension of 201 x 201 grid points on domain, the parameters $\sigma_m \Delta x = 2$ and $\beta = 2$ should be adopted and give good results.

4. Numerical Results

This section presents results of the 1D and 2D wave propagation comparing the DRP, FDo and SO finite difference schemes. The first subsection uses the 1D hyperbolic equation and verify the error with different finite difference schemes. The second subsection presents the effect of the finite difference scheme along the time. The next subsection compare the finite difference schemes effect for a given instant on time comparing the pulse shape. The following section presents the effect of PML on numerical results.

4.1. Analysis and results for finite difference schemes

To analyze the performance of finite difference schemes, its spectrum is analyzed. With the spectrum analysis, the family of wave number where there is transport without significant dispersion can be seen. The region where, the modified wavenumber of a finite difference scheme gives the same value of the wave number, is free of dispersion error. Since only centered schemes are evaluated no dissipation is introduced via finite difference schemes. The spectrum of the schemes and their dispersion error are shown in Figs. 3 and 4, respectively. Observing Figs. 3 and 4 one can note that SO scheme of 11-stencil-points presents almost the same spectral quality of the FDo13p (scheme with 13-stencil-points). Comparing the dispersion error versus number of points-per-wave one can note that for a small number of points-per-wave, says 5, the SO scheme presents a small dispersion error when compared with other schemes showed in present work.

All calculations where carried out, using the formula and the initial conditions given in subsection 2.1. 400 steps were integrated in time, on a non-dimensional domain with length 500. No outflow boundary conditions was added to the code because the information does not reaches this boundary. For each calculation the following discretization constants was adopted: $\Delta t = \Delta x = 1$. This constants implies on a CFL (Courant-Friedrichs-Lewy) number equal to 1. For each calculation performed on present paper the residue error is defined as:

$$E_{RMS} = \sqrt{\sum_{j=1}^{N} \frac{\left(u_j - u'_j\right)^2}{(n-1) \times n}} \tag{23}$$

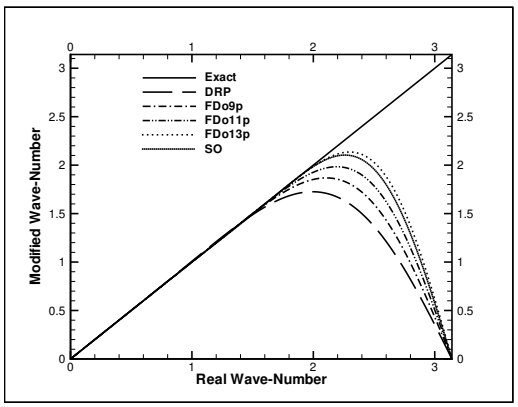

Figure 3: Spectrum of finite difference schemes.

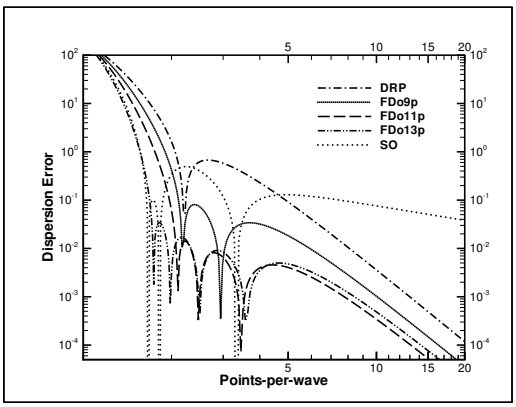

Figure 4: Finite difference dispersion error.

where u_j is the exact solution and u'_j is the numerical result and N is the number of points in the spatial domain. For time integration the traditional fourth-order four steps Runge-Kutta schemes was adopted.

The Tab. 2 presents the E_{RMS} for the DRP, FDo9p, FDo11p, FDo13p and SO finite difference schemes. Analyzing the results present on Tab. 2 it can be seen that for one dimensional wave propagation the SO finite

Table 2: E_{RMS} for the finite difference schemes analyzed at present paper.

Scheme	DRP	FDo9p	FDo11p	FDo13p	SO
E_{RMS}	1.556×10^{-3}	1.701×10^{-3}	1.663×10^{-3}	1.681×10^{-3}	0.847×10^{-3}

difference schemes presents better results when compared with other ones.

4.2. The effect of the finite difference scheme along the time

For this subsection on, the results were obtained using the LEE (subsection 2.2). For all calculations presented on the next subsections the following numerical constants were adopted:

- $\Delta x = \Delta y = 1$;
- $Mach = 0.5$;
- $\Delta t = 1/(1 + Mach)$.

To evaluate numerical results along time the L_2-norm is computed:

$$L_2(t) = \left[\frac{1}{N^2} \sum_{i,j}^{N^2} p'^2_{i,j}(t) \right]^{1/2}, \tag{24}$$

The Fig. 5 presents the L2 norm along the time for the exact solution. This figure is useful to explain how the sound intensity is dissipated, although aeroacoustic problems have no viscosity. Along the time, the propagation of the acoustic wave causes a reduction on its intensity, dissipating the noise. To evaluate along the time the effect of the finite difference scheme on solution along the time the Figs. 6 and 7 presents details of two regions of Fig. 5. Comparing the figures one can note that for all time range there are errors. comparing the results on time 54 to 64 and 95 to 100 one can note that the errors added to the code are improved. Comparing the finite difference results with the exact solution one can note that all finite difference presents similar results. The family of FDo finite difference schemes presents the best results. The results of FDo9p, FDo11p and FDo13p gave almost the same result. The proposed SO scheme has results similar to DRP finite difference scheme present on literature.

4.3. Comparison of finite difference schemes

To compare the real efficiency of finite difference schemes a 2-dimensional pulse propagation was carried out. The results on Figs. 8 and 9 show the general characteristics of the analyzed pulse and the details of the region marked with a circle, respectively. The region marked with a circle in Fig. 8 was chosen for analysis because it is the region that presents the worse results along all domain. Comparing the results that the tested finite

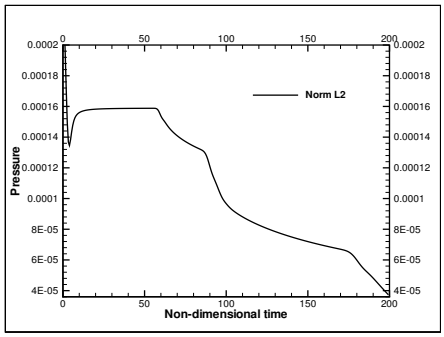

Figure 5: Exact L2 norm along non-dimensional time.

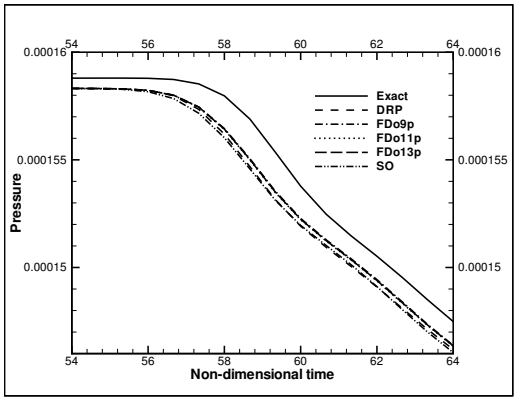

Figure 6: Details of L2 norm on non-dimensional time 54 to 64.

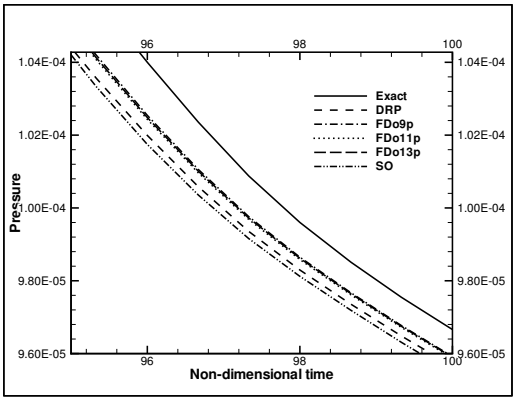

Figure 7: Details of L2 norm on non-dimensional time 95 to 100.

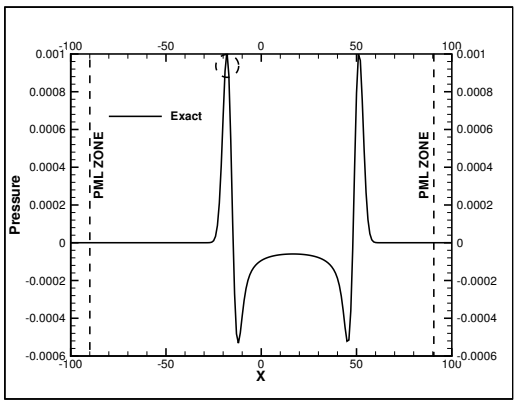

Figure 8: General characteristics of the pulse on t = 50/3.

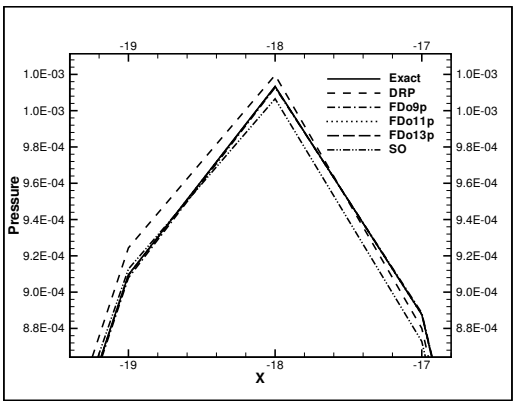

Figure 9: Detail of the pulse on the region marked with a circle of Fig. 8.

difference schemes presents in Fig. 9 one can note that the finite difference schemes FDo9p, FDo11p, FDo13p, presents results almost equal to the exact solution. On other hand the DRP and SO finite difference schemes presents some errors when compared with the exact solution. Comparing these results with the presented in Figs. 3 and 4, one can note that the the errors presented in Fig. 9 can be caused mainly by waves with many points-per-wave. This suggests that a finite difference scheme should not be optimized to transport waves with a great range of points-per-wave, but to transport waves with a small number of points-per-wave, giving a smaller dispersion error in these cases.

4.4. The effect of PML on the main pulse

To analyze the effect of PML on the main pulse the wave propagation is carried out with the same conditions presented on previous sections. The 11 points SO scheme was used for the calculations of the spatial derivatives.

A first study is done with the intention to characterize the need of the PML zone coupled with the physical

boundary conditions of the problem. The Figs. 10 and 11, presents respectively, the pulse propagation on time $t = 400/3$. The left figure shows a case that there is no application of the PML zone and the right presents a figure where this zone is added to the numerical code. Comparing the figures one can note that the pulse

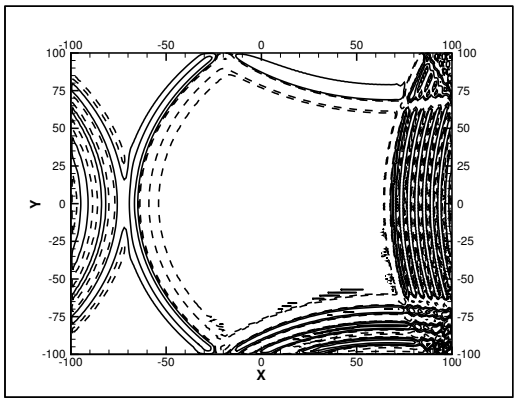

Figure 10: Wave transport with the physical boundary condition but without PML region.

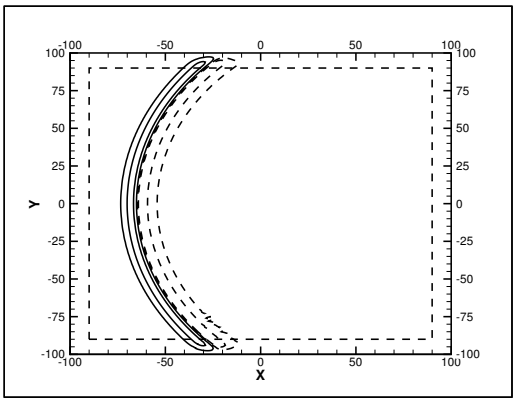

Figure 11: Wave transport with physical boundary condition and PML region.

transport without the use of PML zone implies on a very reflective boundary. These reflections do not represent the physical condition of a rigid wall reflection, they are only numerical spurious reflections.

In order to analise the effects of the PML zone, two simulations were carried out, changing width and height of the computational domain. This was done by using a domain with 201 x 201 points and another with 401 x 401 points. The results after integrating some steps in time for both simulations are shown if Figs. 12 and 13. Fig. 13 shows the details of the region that is marked with a circle in Fig. 12. Observing the Fig. 13 one can

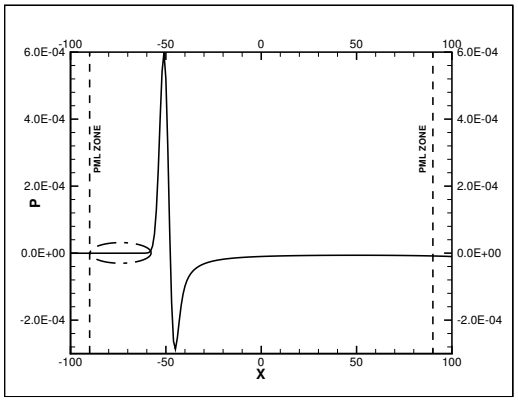

Figure 12: General characteristics of the analyzed pulse.

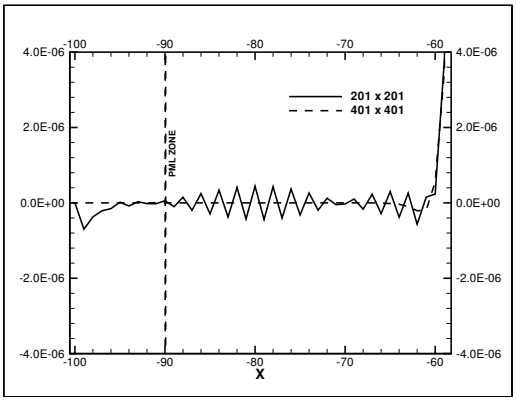

Figure 13: Detail of the circled region on the left figure.

note that the boundary introduces a perturbation error on the order of error of 1.0×10^{-7}, while the intensity of the main pulse is on the order of 1.0×10^{-4}. Comparing the relation of intensity on can note that the intensity of the main pulse on the order of 1000 times greater than the perturbations. This amplitude is acceptable for most of the cases studied.

To analyze the effect of the number of points on PML zone, three different number of points were adopted in the PML region: 6, 10 and 16 points. The simulations were integrated 150 steps in time. The numerical results are shown in Fig. 14 and its details showed in Fig. 15. The results presented on Fig. 15 shows that for 6 points on PML zone there is an introduction of a error, when the solution is compared with the exact. For transports with 10 and 16 points in the PML zone, one can note that the both solutions gave almost the same result. This result coupled with the presented on Fig. 13 lead to the conclusion that for square domains with more than 201 x 201 points, 10 points on PML zone is enough.

5. Conclusions

In this paper a review and comparison of the DRP, FDo, and a new finite difference scheme, based on spectral optimization – SO schemes were done. The 1D results showed that, for a sine function propagation, the SO scheme has the lowest error if compared with the others. A LEE code was used for a 2D verification. For this

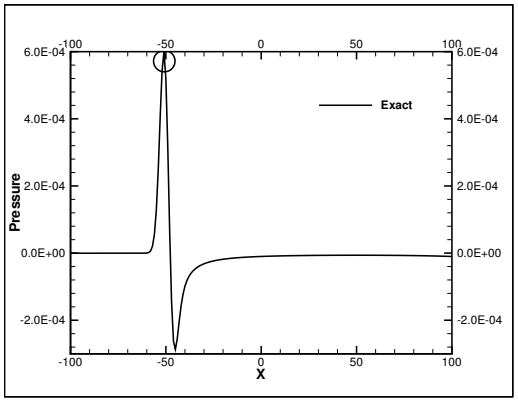

Figure 14: General view of the pulse used to analyze the effect of the number of point on PML zone.

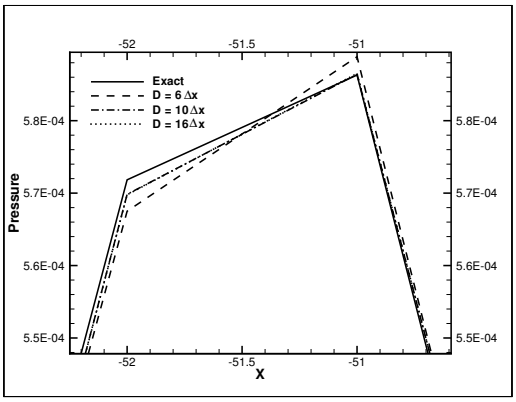

Figure 15: Detail of the left figure.

verification a benchmark case of a Gaussian pulse propagation was performed. In these cases the FDo schemes were better than the others. The result obtained with SO scheme in this case was almost the same of the DRP scheme. An analisys of the SO scheme accoupled with 4th order Runge-Kutta scheme showed that this scheme can be unstable for CFL > 1.3. As boundary conditions the non-reflective Perfectly Matched Layer (PML) zone was implemented and analyzed. The analysis of the PML zone shows that the reflections are of order 0.1% of the maximum wave amplitude, and therefore is a good technique to avoid reflections at the boundaries.

6. Acknowledgments

The authors acknowledge the financial support given by FAPESP under grants 05/00001-0 and 04/07507-4.

7. References

Bogey, C. and Bailly, C., 2004, A Family of Low Dispersive and Low Dissipative Explicit Schemes for Flow and Noise Computation, "Journal of Computational Physics", Vol. 194, pp. 194–214.

Colonius, T., Lele, S. K., and Moin, P., 1993, Boundary Conditions for Direct Computation of Aerodynamic Sound Generation, "AIAA Journal", Vol. 31, pp. 1574–1582.

Curle, J., 1955, The Influence of Solid Boundaries Upon Aerodynamic Sound, "Proc. Roy. Soc.", Vol. 231, pp. 505–514.

Hu, F. Q., 1996, On Absorbing Boundary Conditions for Linearized Euler Equations by a Perfectly Matched Layer, "Journal of Computational Physics", Vol. 129, pp. 201–219.

Hu, F. Q., 2001, A Stable, Perfectly Matched Layer for Linearized Euler Equations in Unsplit Physical Variables, "Journal of Computational Physics", Vol. 173, pp. 455–480.

Lele, S. K., 1992, Compact Finite Differences Schemes with Spectral-like Resolution, "Journal of Computational Physics", Vol. 103, pp. 16–42.

Lighthill, M. J., 1952, On Sound Generated Aerodynamically, i. general theory, "Proc. Roy. Soc.", Vol. 211, pp. 564–587.

Lighthill, M. J., 1954, On Sound Generated Aerodynamically, ii. turbulence as source of sound, "Proc. Roy. Soc.", Vol. 222, pp. 1–32.

Tam, C. K. W., 1995, Computational Aeroacoustics: Issues And Methods, "AIAA Journal", Vol. 33, pp. 1788–1796.

Tam, C. K. W. and Webb, J. C., 1993, Dispersion-Relation-Preserving Finite Difference Schemes for Computational Acoustics, "Journal of Computational Physics", Vol. 107, pp. 262–281.

Williams, J. E. F., 1963, The Noise from Turbulence convected at High Speed, "Philos. Trans. Roy. Soc.", Vol. 255, pp. 496–503.

Williams, J. E. F., 1969, Sound Generation by Turbulence and surfaces in Arbitrary Motion, "Philos. Trans. Roy. Soc.", Vol. 264, pp. 321–342.